Geophysical Research Letters

RESEARCH LETTER
10.1029/2025GL117836

Global Occurrence of Kelvin-Helmholtz Vortices at Mars

Ze-Wen Koh[1,2,3], Gangkai Poh[2,3], Christopher M. Fowler[4], Kathleen Gwen Hanley[5], Xuanye Ma[6], Jacob R. Gruesbeck[3], Dona Chathuni P. Kuruppuaratchi[3,7], Weijie Sun[5], Gina A. DiBraccio[8], and Jared Randolph Espley[3]

[1]Department of Earth, Atmospheric and Planetary Sciences, Massachusetts Institute of Technology, Cambridge, MA, USA, [2]Center for Research and Exploration in Space Sciences and Technology II, Catholic University of America, Washington, DC, USA, [3]Solar System Exploration Division, NASA Goddard Space Flight Center, Greenbelt, MD, USA, [4]Department of Physics and Astronomy, West Virginia University, Morgantown, WV, USA, [5]Space Sciences Laboratory, University of California, Berkeley, Berkeley, CA, USA, [6]Center for Space and Atmospheric Research and Physical Sciences Department, Embry-Riddle Aeronautical University, Daytona Beach, FL, USA, [7]Department of Astronomy, University of Maryland, College Park, MD, USA, [8]Heliophysics Science Division, NASA Goddard Space Flight Center, Greenbelt, MD, USA

Key Points:

- We observed the first fully developed K-H vortices at Mars' southern hemisphere and equatorial flanks, indicating a global distribution
- Heavy planetary ions reduce growth rates, but increase the solid angle that is K-H unstable, suggesting a higher occurrence frequency
- Inferred higher occurrence rates over a larger spatial region imply higher atmospheric loss rates from detached clouds than prior estimates

Correspondence to:
Z.-W. Koh,
kohzewen@mit.edu

Citation:
Koh, Z.-W., Poh, G., Fowler, C. M., Hanley, K. G., Ma, X., Gruesbeck, J. R., et al. (2025). Global occurrence of Kelvin-Helmholtz vortices at Mars. *Geophysical Research Letters*, *52*, e2025GL117836. https://doi.org/10.1029/2025GL117836

Received 27 JUN 2025
Accepted 5 NOV 2025
Corrected 10 DEC 2025

This article was corrected on 10 DEC 2025. See the end of the full text for details.

Abstract We analyzed six Kelvin-Helmholtz (K-H) vortex events from Mars Atmosphere and Volatile EvolutioN (MAVEN) measurements. We found that fully developed vortices can occur at Mars' equatorial flanks and in the southern hemisphere, while they were previously observed only in the northern hemisphere. This implies that they do not exhibit a hemispheric asymmetry, and may occur globally as long as onset conditions are satisfied. We also estimated growth rates of 10^{-3}–10^{-2} s^{-1}, and found that the inclusion of heavy planetary ions reduces growth rates while increasing the directions over which K-H instability occurs. We calculated instantaneous ion loss rates due to detachment of K-H vortices of 10^{25}–10^{27} s^{-1}, rivaling other loss mechanisms in contributing to Mars' global atmospheric escape. The inferred higher occurrence rate of K-H instability at Mars over a larger spatial domain strongly suggests a more significant contribution to overall atmospheric loss than previously thought.

Plain Language Summary When solar wind from the Sun meets the magnetic field of Mars, it slows down significantly. This difference in plasma speed can induce vortices to form at the boundary of Mars' magnetic field, called "Kelvin-Helmholtz (K-H) vortices." These vortices are important because when they fully develop, they can break off from the boundary and contribute to the loss of Mars' atmosphere. We used satellite data to identify six fully developed K-H vortices. While they have previously only been found in the northern hemisphere, our study found for the first time that they also occur at the equator and in the southern hemisphere, proving that they are a global phenomenon. We estimated the growth rate of the vortices, and found that heavy planetary ions from Mars like oxygen can cause K-H vortices to grow slower, but ultimately increase the directions in which they can occur. Finally, we calculated atmospheric loss rates caused by K-H vortices, and found that they are comparable to other loss mechanisms in contributing to Mars' atmospheric escape.

1. Introduction

The Kelvin-Helmholtz (K-H) instability occurs due to a velocity shear at the boundary between two fluids (Chandrasekhar & Gillis, 1962), and is well-known to occur at the interface between the solar wind and globally magnetized planets like Mercury (Boardsen et al., 2010; Sundberg et al., 2011), Earth (Fairfield et al., 2000; Hasegawa et al., 2004; Taylor et al., 2012), and Saturn (Delamere et al., 2013; Masters et al., 2010, 2012). The K-H instability is also thought to occur at non-magnetized planets due to the direct interaction between the solar wind and the planet's ionosphere, leading to the formation of partially and fully developed vortices. One well-studied example is Venus, where observations (Brace et al., 1982) and numerical simulations (Amerstorfer et al., 2010; Terada et al., 2002; Thomas & Winske, 1991) have concluded that K-H vortices can develop along the Venusian ionopause.

Mars presents a unique case as a non-magnetized planet that has remnant crustal magnetic fields, the strongest of which are located in the southern hemisphere. Since the launch of the Mars Atmosphere and Volatile EvolutioN (MAVEN) mission (Jakosky et al., 2015), individual instances of partially (Ruhunusiri et al., 2016) and fully developed K-H (Poh et al., 2021; X. Wang et al., 2022) vortices have since been observed at the Martian induced magnetospheric boundary (IMB). However, the scale, properties, and distribution of K-H vortices at Mars are still

poorly constrained; their formation and evolution remain an open question. Fully developed K-H vortices can detach as plasma clouds, leading to the escape of atmospheric ions such as oxygen (Dang et al., 2022; Wolff et al., 1980). Previous models and empirical case studies have shown that atmospheric loss due to K-H vortices could rival other known loss mechanisms such as atmospheric sputtering, photochemical processes, and ion pickup. Hence, establishing how and where K-H vortices occur is critical to better constraining the rate of Mars' atmospheric escape.

In this work, we present a multi-event case study of six fully developed K-H vortices, identified from MAVEN observations by their characteristic magnetic field and plasma signature. We estimated key metrics of interest for the events observed such as their distribution, onset conditions, growth rate, and mass loss rate. Hybrid simulations (Delamere et al., 2011, 2021) have shown that heavy ions could play a significant role in decreasing growth rates, as the ion inertial length increases linearly with mass, and the inclusion of heavies like oxygen could lead to the suppression of wavelengths less than the ion inertial length. Hence, we also assess the effect of the inclusion of heavy ions on growth rates at Mars. To our knowledge, this study presents for the first time vortices found in both hemispheres and at the equatorial flanks, indicating a global distribution at Mars.

2. Methods

In this study, we used MAVEN magnetic field and plasma measurements to visually identify events representing best-case examples of fully developed K-H vortices at Mars. We conducted a brief, initial 7-month survey from January to July 2018, followed by surveys in September 2019 and October 2022. The data set used includes MAVEN's Magnetometer (MAG, Connerney et al., 2015), Solar Wind Electron Analyzer (SWEA, Mitchell et al., 2016), Solar Wind Ion Analyzer (SWIA, Halekas et al., 2015), and SupraThermal And Thermal Ion Composition (STATIC, McFadden et al., 2015) instruments. An overview of the observations is presented in Figure 1. In the following analysis, we use Mars Solar Orbital (MSO) coordinates, where the x-axis points sunward from Mars, the y-axis points opposite to the Martian orbital velocity, and the z-axis completes the right-handed coordinate system.

2.1. Identification Criteria for K-H Vortices

The characteristic magnetic field and plasma signature of fully developed K-H vortices include (a) quasi-periodic, sawtooth-like perturbations in the magnetic field, (b) a corresponding decrease in ion density, (c) a tailward enhancement in ion velocities, (d) the coexistence of magnetosheath and plasma populations within the mixing region of the vortex, and (e) a pressure enhancement at the edge of the vortex with a minimum at its center, such that the pressure increase satisfies the inequality condition $\Delta P \geq \frac{1}{2}\rho(\Delta v)^2$, where ΔP is the pressure increase, ρ is the ion density, and Δv is the flow shear (Hasegawa, 2012; Poh et al., 2021). To illustrate our methodology for identification, we present as a case study an event that occurred on 21 September 2019 between 22:25:00 and 22:55:00 UTC (Figure 1), noting that the other five events similarly exhibit all criteria outlined. This event occurred at a solar zenith angle approaching 90∘, as the spacecraft skimmed parallel to the IMB and experienced a velocity shear.

The observed interval starts with the spacecraft in the Martian induced magnetosphere. The induced magnetosphere can be easily identified in Figures 1o and 1p by the presence of planetary heavy ions such as O^+ and $O_2{}^+$ as well as in Figures 1m and 1n by the cold (<10 eV) planetary protons in both SWIA and STATIC H^+ energy spectrograms. Between 22:30:00 and 22:55:00 UTC, the spacecraft encountered the IMB, as can be seen from the gradual decrease in the magnetic field magnitude $|\mathbf{B}|$ from ∼10 to ∼2.5 nT. By the end of the interval, MAVEN has entered the magnetosheath region, as shown by the highly turbulent, high frequency fluctuations in $|\mathbf{B}|$, and more notably, the presence of high energy protons between 10^2 and 10^3 eV and the lack of planetary heavy ions.

In the transition from Mars' induced magnetosphere to the magnetosheath, MAVEN observed a significant increase in tailward H^+ velocity (Figure 1j) from ∼100 to ∼250 km s^{-1}. This velocity shear across the IMB is highly conducive for K-H instabilities. The development of K-H vortices at the boundary is evidenced by the quasi-periodic, bipolar, sawtooth-like perturbations that MAVEN observed in the magnetic field data (outlined in Figure 1 with dashed lines), most significantly in B_x and B_y. B_x and B_y are observed to undergo anti-correlated spikes in magnitude and polarity at each wave cycle, such that minima in B_x correspond to maxima in B_y and vice versa. This sawtooth-like perturbation is characteristic of K-H vortices, serving as a signature for their

10.1029/2025GL117836

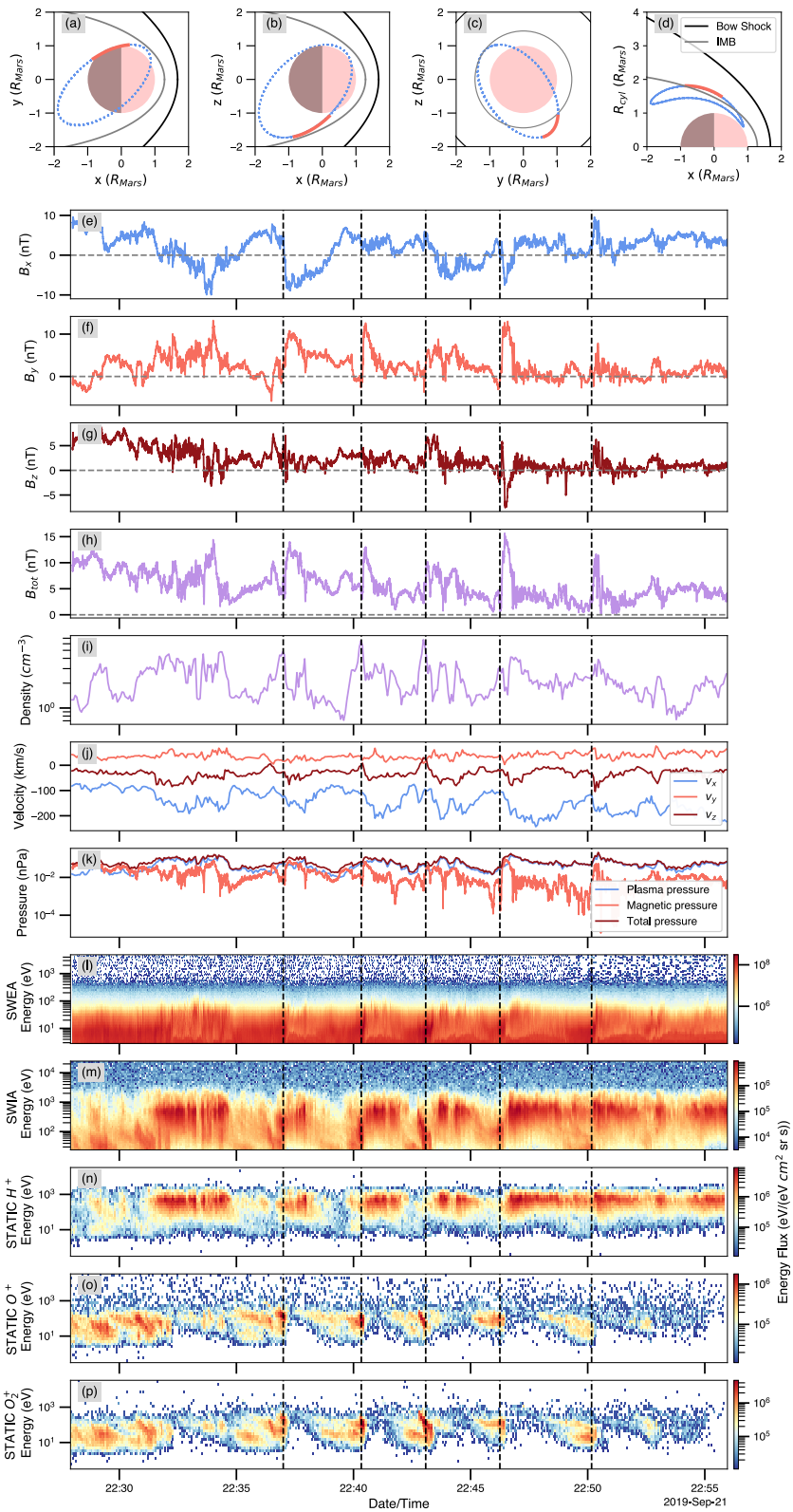

Figure 1.

identification in previous work at Earth (e.g., Fairfield et al., 2000; Hasegawa et al., 2004). The magnetic field perturbations are accompanied by oscillations in plasma measurements, including decreases in ion density aligning with the bipolar signature (Figure 1i). As such, the signature encountered by the spacecraft strongly indicates a wave train of fully developed K-H vortices.

Further evidence can be found by examining the SWIA H^+ and STATIC H^+, O^+, and $O_2{}^+$ energy spectrograms (Figures 1m–1p). We find that the perturbations above coincide with periodic increases in the detection of cold planetary protons and heavy ions, aligning with the spine of each vortex, against a background of hotter planetary protons and an absence of heavy ions. This signature is strongly characteristic of the mixing of magnetosheath and planetary plasma populations within the vortex structure. The periodicity of the detected planetary ions aligns perfectly with the sawtooth-like oscillations observed in the magnetic field, proving it highly likely that the event observed is a wave train of K-H vortices.

The sawtooth-like magnetic field signature of K-H vortices shares some similarities with the bipolar signature of magnetic flux ropes (Russell & Elphic, 1979). However, magnetic flux ropes are uniquely distinguished by a strong enhancement in $|\mathbf{B}|$ along the axis of the flux rope, coinciding with the center of the bipolar signature (DiBraccio et al., 2015), which K-H vortices do not exhibit. Besides the enhancement in $|\mathbf{B}|$, magnetic flux ropes relatedly exhibit maximum total pressure at the center of the bipolar signature, where their core field is. K-H vortices instead experience a minimum in total pressure at the center of the vortex, and a maximum at the edge (e.g., as seen in the close-up view in Figure 2 at 22:43:40 UTC), due to centrifugal motion pushing out plasma from the center of the vortex (Hasegawa, 2012; Hasegawa et al., 2009; Kavosi & Raeder, 2015). We found that this is the case for the perturbations observed in this study. Additionally, the pressure enhancements at the edge of the vortices follow the inequality condition $\Delta P \geq \frac{1}{2}\rho(\Delta v)^2$ on order of magnitude; this indicates that the K-H vortex is rolled up and in the nonlinear stage (Hasegawa, 2012).

Interestingly, MAVEN also observed signatures of planetary ion energy dispersion, indicated by the detection of fast, high energy ions before encountering slower and colder ions near the leading edges of the vortices. This observation appears to indicate the occurrence of ion acceleration and energization at the edges of the vortices. Energy dispersion of heavy ions has previously been observed at Mars due to detached plasma clouds, and was postulated to reflect an escape mechanism known as the "snowplow" effect (Halekas et al., 2016) caused by momentum transfer between solar wind protons and heavy planetary ions. Our finding implies that K-H vortices may be an alternative cause of planetary ion energy dispersion, indicating that observed energy dispersion events must be closely examined to determine their exact source mechanism. The waves in this study were determined not to be snowplows from the criteria above, as well as observations of large planetary ion fluxes coinciding with the magnetic field perturbations.

2.2. Minimum Variance Analysis

In addition to the signatures outlined above, we can distinguish between the morphologies of K-H vortices and magnetic flux ropes using minimum variance analysis (MVA) (Sonnerup & Scheible, 1998). Figure 2 illustrates a close-up view of our case study event between the times of 22:42:00 and 22:48:00 UTC. By applying MVA on the second bipolar signature at 22:40:20, our hodogram results (Figure 2, right column) indicate that there is little variation in the minimum and intermediate variance directions, B_{min} and B_{int}, as compared to the maximum variance direction B_{max}. The MVA results were found to be similar across all sawtooth-like signatures in the wave train. This signature is characteristic of a boundary layer or current sheet crossing, as is typical for a K-H vortex. Conversely, the MVA hodogram of a magnetic flux rope is associated with a clear bipolar rotation of the magnetic field. This is caused by a bipolar signature in the maximum variance direction and a peak in the intermediate direction—associated with the core field—which are absent in this event (e.g., Figure 1c in Smith et al., 2017). Finally, the ratio of the intermediate to minimum eigenvalue is 17.7 in this case (and largely found to be ≥3 for all vortices), indicating that the constructed boundary normal direction is reliable and the structure encountered is

Figure 1. The top panel shows Mars Atmosphere and Volatile EvolutioN's orbit on 21 September 2019 in the (a) equatorial, (b) noon-midnight, (c) terminator, and (d) cylindrical plane respectively, where the red line indicates the time interval shown in the bottom panels. Panels (e–h) show the *x*-, *y*-, and *z*-components as well as magnitude of the magnetic field measured by the Magnetometer. Panels (i–k) show the ion moments measured by Solar Wind Ion Analyzer (SWIA), followed by the energy spectrograms of (l) electrons measured by Solar Wind Electron Analyzer and (m) protons from SWIA. Panels (n–p) show SupraThermal And Thermal Ion Composition energy spectrograms of H^+, O^+, and $O_2{}^+$ ions. The black dashed lines in all panels represent the center of the sawtooth-like signatures.

10.1029/2025GL117836

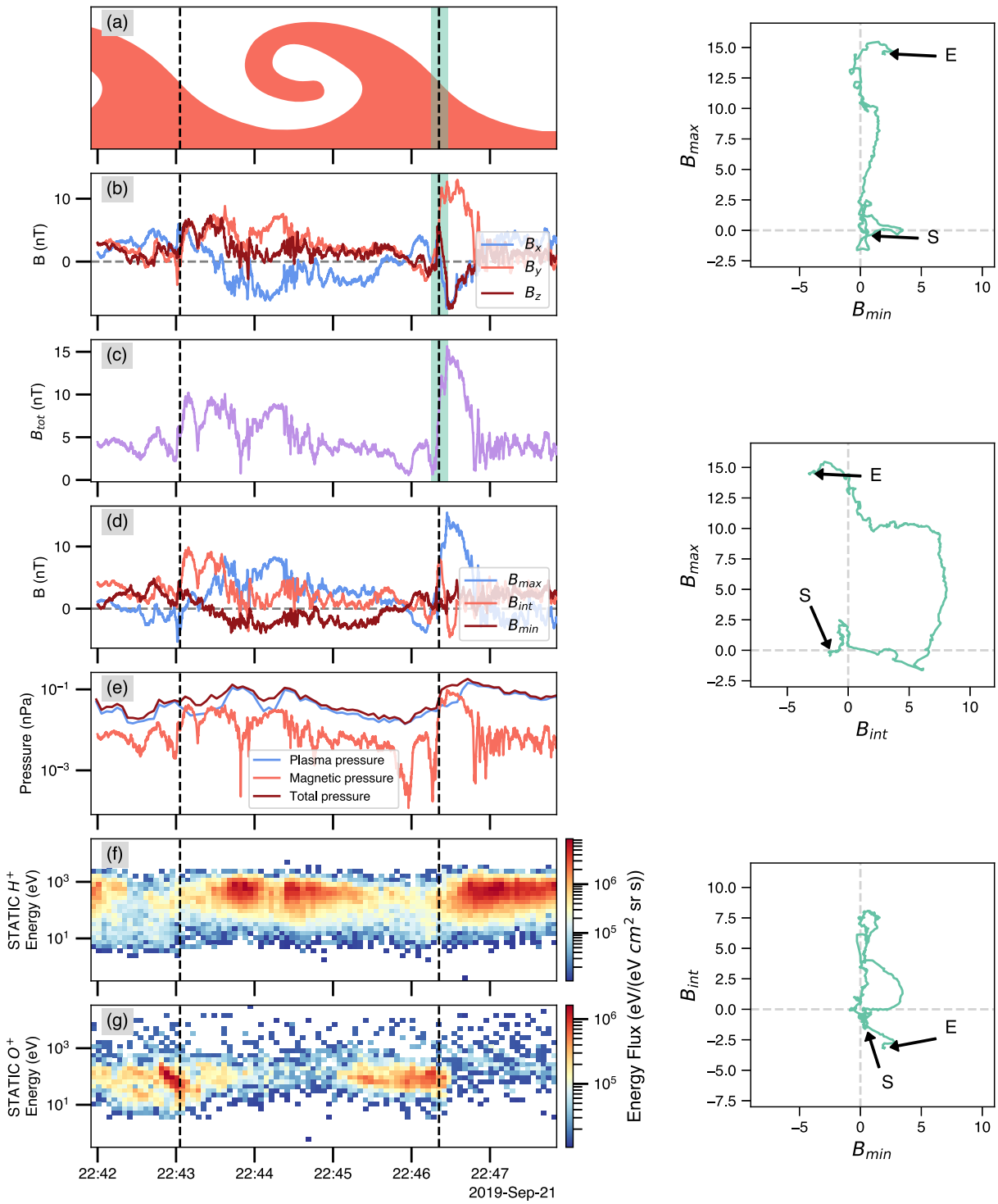

Figure 2. In the left column, panel (a) shows a schematic of a K-H wave train as interpreted from Mars Atmosphere and Volatile EvolutioN measurements, whereas panel (b) shows the *x*-, *y*-, and *z*-component of the magnetic field measurement and panel (c) shows its corresponding magnitude. In all three panels, the teal highlighted region represents the center of the sawtooth-like signature that is used for minimum variance analysis (MVA). Panel (d) shows the magnetic field components in the maximum, intermediate, and minimum variance directions. Panel (e) shows pressure as measured by the Magnetometer and Solar Wind Ion Analyzer, and panels (f, g) show respectively the energy spectrograms of H^+ and O^+ ions as measured by SupraThermal And Thermal Ion Composition. The right column shows the MVA hodogram of the highlighted interval. The characters "S" and "E" indicate the start and end of the vector.

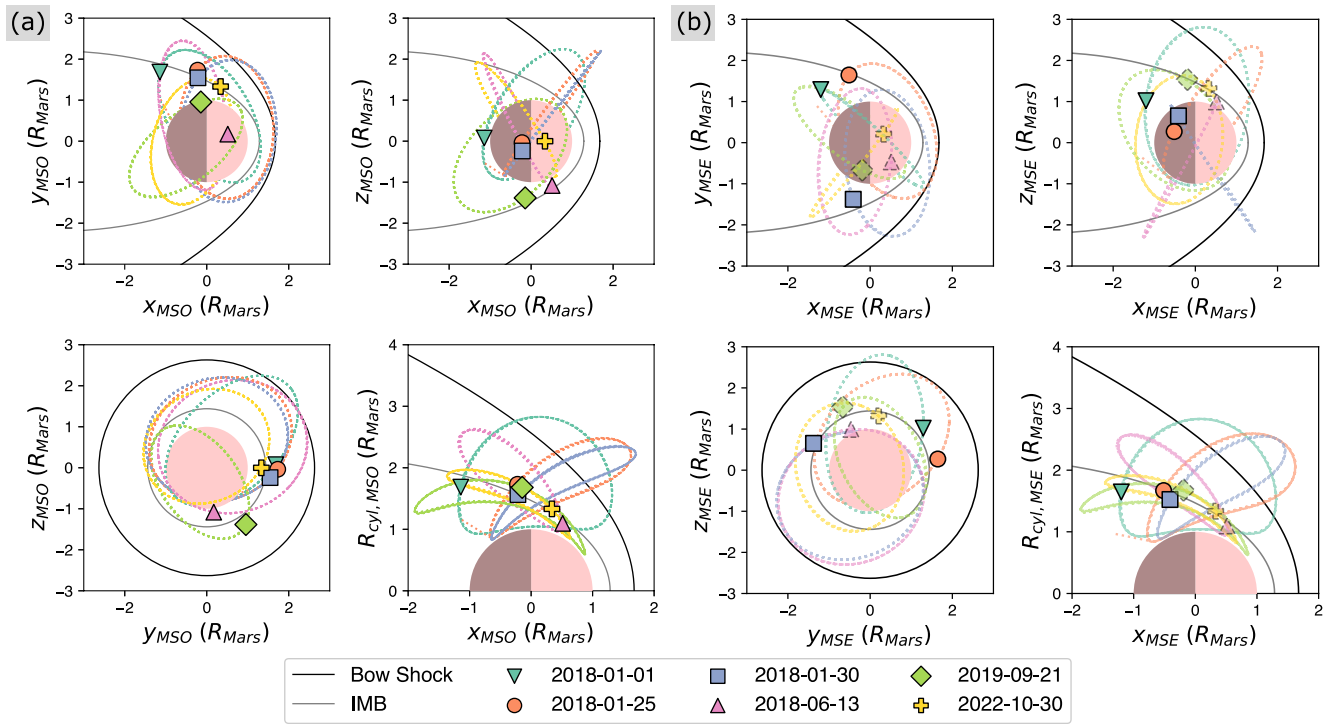

Figure 3. The distribution of the six K-H vortex intervals identified in this work presented in (a) Mars Solar Orbital coordinates and (b) Mars Solar Electric coordinates, shown in the *x*-*y* plane (top left), *x*-*z* plane (top right), *y*-*z* plane (bottom left), and in the cylindrical plane (bottom right). Mars is shown by a pink circle. The symbols indicate each vortex event observed, with the dotted line in corresponding colors representing Mars Atmosphere and Volatile EvolutioN's orbit during the observation.

likely a boundary layer crossing (Boardsen et al., 2010; Sonnerup & Scheible, 1998; X. Wang et al., 2022). Note that the eigenvalue ratio corresponds to the local boundary along the spine of the K-H vortex, not the global boundary normal coordinates. Overall, the MVA results corroborate our hypothesis that MAVEN encountered a wave train of rolled-up K-H vortices, and not a magnetic flux rope.

3. Multi-Event Analysis and Results

In this multi-event study, we analyzed six intervals during which MAVEN observed a train of K-H vortices. These events are selected best-case examples of K-H vortices observed at Mars, and do not represent a comprehensive survey of the MAVEN data. The six K-H vortex intervals were observed at solar zenith angles between 70∘ and 135∘, with peak-to-peak amplitude and time separations of ∼5–25 nT and ∼0.5–3.5 min, respectively. Previous magnetohydrodynamic (MHD) simulations have indicated that K-H waves propagate at a velocity between the average and center-of-mass velocities, $(\mathbf{v}_1 + \mathbf{v}_2)/2$ and $(\rho_1\mathbf{v}_1 + \rho_2\mathbf{v}_2)/2$, where the subscripts 1 and 2 refer to parameters on either side of the flow shear boundary (Hasegawa et al., 2009). Assuming that the velocity of the K-H waves are the average of these two values as in Ruhunusiri et al. (2016), we determined that the K-H velocities range between ∼85 and 260 km s^{-1}, with characteristic K-H wavelengths λ (velocity × wave period) varying between ∼3,000 and 34,000 km.

3.1. Boundary of K-H Instability Occurrence

Figure 3a shows the occurrence location of the six K-H intervals in MSO coordinates, where each colored symbol represents a K-H wave train and the corresponding dotted lines show MAVEN's orbit at the time of the observation.

To the best of our knowledge, this work presents the first report of fully developed K-H vortices observed along Mars' IMB at both the equatorial flanks and southern hemisphere. Previously, only partially developed K-H waves have been reported in the southern hemisphere (Ruhunusiri et al., 2016), which was initially thought to be inconducive for nonlinear K-H vortex growth. It was hypothesized that the interactions between the

interplanetary magnetic field (IMF) and Mars' crustal magnetic field in the southern hemisphere could potentially inhibit K-H growth by stabilizing the boundary layer (Poh et al., 2021), while recent case studies (e.g., L. Wang et al., 2023) reported K-H vortices occurring only in the northern hemisphere. However, our results suggest otherwise and indicate that our understanding of the occurrence and onset of K-H instability at Mars must be reexamined.

Additionally, four events were observed at the equatorial flanks of Mars. One of these events occurs downstream from the terminator plane (01 January 2018), while the remaining events occur near the terminator. Interestingly, the equatorial events appear clustered at the dusk flank or in the $+\hat{\mathbf{y}}$-direction (Figure 3a, *y*-*z* plane) as opposed to the dawn flank, although further statistics are required to determine any dawn-dusk asymmetries in K-H onset. Our findings are in strong agreement with previous simulations (Penz et al., 2004), which found that both the polar terminator (under medium solar wind conditions, i.e., $\mathbf{V}_{SW} \sim 400$ km s^{-1}) and equatorial flanks are K-H unstable. Given that solar wind velocity was significant during each event (320–400 km s^{-1}), it is highly likely that the equatorial IMB was unstable to K-H instability in the 13 June 2018 and 21 September 2019 events. The vortices likely became fully "rolled up" at or downstream of the terminator.

To investigate the distribution in the natural reference frame of the induced magnetosphere, we performed a coordinate transformation into the Mars Solar Electric (MSE) coordinate system (DiBraccio et al., 2017; L. Wang et al., 2023), where $\hat{\mathbf{x}}_{MSE}$ is antiparallel to the solar wind flow ($\mathbf{V}_{SW}$), $\hat{\mathbf{z}}_{MSE}$ is parallel to the solar wind convection electric field $\mathbf{E}_{SW} = -\mathbf{V}_{SW} \times \mathbf{B}_{IMF}$, and $\hat{\mathbf{y}}_{MSE}$ completes the right-handed coordinate system. Since MAVEN does not cross into the solar wind for three of the six analyzed orbits (i.e., 13 June 2018, 21 September 2019, and 30 October 2022), we used machine learning-derived estimates of solar wind parameters from Azari et al. (2024) for these events. We include these estimates in Figure 3b for completion (shown in translucent color with dotted edges); however, we note that large spatial uncertainties preclude us from treating these locations as conclusive. Hence, the distribution can only be transformed accurately into MSE coordinates for the remaining three events (i.e., 01 January 2018, 25 January 2018, and 30 January 2018), for which $\mathbf{V}_{SW}$ and $\mathbf{B}_{IMF}$ can be determined.

In previous observations of partially and fully developed K-H vortices, events have been exclusively identified in the −E hemisphere (or $-\hat{\mathbf{z}}_{MSE}$ hemisphere), leading to the hypothesis that there exists a hemispheric asymmetry caused by the gradual piling up of magnetic fields along the +E direction (L. Wang et al., 2023). However in this study, all of the three events (for which we have MAVEN observations of the solar wind) occur in the +E hemisphere (Figure 3b). This novel result implies that the proposed mechanism may not fully explain the excitation of K-H waves. Instead, our observations suggest that there might not exist a hemispheric asymmetry, or a less significant one than initially thought.

The findings above significantly challenge our prior understanding of where the K-H unstable boundary is situated along the Martian IMB. Combined with observations from previous studies, it is clear that there are no limitations on where K-H instabilities may occur. Instead, we require greater understanding on which regions are more (or less) susceptible to the onset and growth of K-H instability. This poses major implications for our current understanding of K-H instability at unmagnetized planets, specifically its onset, growth, and contribution to overall atmospheric loss.

3.2. Onset Conditions and Growth Rate

We examined the observed solar wind and IMF conditions for each event (Table 1). Similar to Earth, the occurrence of K-H vortices in all events are associated with a strong flow shear—particularly in the tailward direction—along the induced magnetospheric (or K-H unstable) boundary, which is necessary for K-H growth. We also observed high densities of O^+ and $O_2{}^+$ relative to proton densities at the induced magnetosphere side of the flow shear boundary, as expected. Such boundary conditions with the asymmetrical presence of heavy ions are unique to unmagnetized planets and has been thought to play an important role in the development and growth of K-H instability.

Importantly, we note that a significant tangential (i.e., B_x, B_y for equatorial flanks and B_x, Bz for polar events), draped magnetosheath magnetic field was observed for most of the events, excepting the 30 January 2018 observation. This differs from our prior understanding at Earth, where a strong tangential draped magnetic field along the flow shear boundary is thought to stabilize K-H instability modes. However, more recent work at Earth

Geophysical Research Letters

10.1029/2025GL117836

Table 1
Solar Wind and Interplanetary Magnetic Field Conditions for K-H Vortex Intervals

Date	Most unstable direction	λ (10^3 km)	γ (s^{-1})	Ω_{KH} (%)	Loss rate (s^{-1})	Region	B (nT)	v_{H^+} (km/s)	n_{H^+}[a] (cm^{-3})	n_{O^+} (cm^{-3})	$n_{O_2^+}$ (cm^{-3})
01 January 2018	[−1.00, 0.00, 0.00]	15.49	3.63×10^{-3}	69	3.66×10^{25}	MSH[b]	[−4.36, 1.73, −3.01]	[−185.68, −28.49, −64.43]	2.59	0.05	0.21
						IM[c]	[7.42, −3.10, −0.59]	[−99.42, −19.75, −15.43]	0.77	2.08	12.53
25 January 2018	[−0.73, 0.68, 0.01]	12.92	1.95×10^{-2}	66	1.39×10^{25}	MSH	[−3.96, 2.38, −0.56]	[−206.42, 103.92, −45.07]	2.82	0.03	0.10
						IM	[−7.72, 0.39, −3.73]	[−76.22, 2.61, −13.94]	0.16	0.30	1.30
30 January 2018	[−0.83, 0.56, 0.04]	32.82	2.03×10^{-2}	74	5.10×10^{26}	MSH	[−4.44, 1.70, 7.14]	[−286.12, 171.62, 29.25]	5.52	0.03	0.08
						IM	[6.99, 4.36, 0.33]	[−73.27, 1.04, 31.87]	0.23	2.53	4.24
13 June 2018	[−0.96, −0.15, −0.21]	2.96	1.37×10^{-2}	26	1.84×10^{25}	MSH	[8.62, −4.76, 5.75]	[−112.35, 21.60, −41.74]	8.59	0.15	0.10
						IM	[3.45, −15.7, −4.45]	[−17.53, 3.01, 42.04]	1.47	23.19	68.42
21 September 2019	[−0.87, 0.35, 0.35]	32.80	1.93×10^{-3}	41	1.24×10^{27}	MSH	[3.50, 0.83, 0.74]	[−211.00, 55.90, −29.49]	1.95	0.05	0.06
						IM	[6.93, −0.17, 7.53]	[−87.63, 39.33, −32.84]	1.47	4.63	9.62
30 October 2022	[−0.94, −0.01, 0.34]	34.41	2.85×10^{-3}	66	7.57×10^{26}	MSH	[6.22, −4.58, 2.40]	[−202.87, 72.05, 26.05]	7.51	0.09	0.07
						IM	[16.98, −7.62, −0.37]	[−81.86, −9.57, 35.75]	0.37	6.44	22.68

[a]Number density of ions, where subscript indicates ion species. [b]Magnetosheath. [c]Induced magnetosphere.

(e.g., Adamson et al., 2016; Ma, 2023; Nykyri et al., 2006) has demonstrated that a strong tangential magnetic field may not necessarily stabilize the K-H instability. This is because the $\boldsymbol{k}$-vector can "orient" itself obliquely away from plasma flow, such that conditions become conducive for K-H onset. Given in addition the evidenced observations in this study, this indicates that the boundary in question is indeed unstable to K-H instability modes.

Furthermore, using the methodology of Ma (2023), we determined for all events the most K-H unstable direction, growth rate γ, and solid angle Ω_{KH} over which instability can occur (i.e., $\gamma^2 > 0$). This approach yields comparable results to alternative single (Boardsen et al., 2010; Eriksson et al., 2016; Hasegawa, 2012) and multi-spacecraft (Blasl et al., 2022) methods for determining $\boldsymbol{k}$. Note that a given perturbation can contain wave vectors $\boldsymbol{k}$ in all directions, but that the K-H mode with the highest γ becomes the dominant mode. Overall, we find that the dominant K-H unstable directions primarily point in the $-\hat{\mathbf{x}}$ or tailward direction, aligning with the strongest flow shear. Growth rates in the most K-H unstable direction range between 10^{-2} and 10^{-3} s^{-1}, agreeing with previous modeled (10^{-2} s^{-1}, Penz et al., 2004) and empirical (10^{-3} s^{-1}, Poh et al., 2021) calculations. We also find that the solid angle over which K-H instability can occur covers ~26%–74% of the entire field-of-view (i.e., 4π steradians). In fact, in the majority of events, K-H onset is possible in >65% of the field-of-view. Note that we did not observe an obvious correlation between Ω_{KH} and γ. Our analysis demonstrates the "ease" of K-H onset at Mars, given the wide angular range wherein K-H modes can grow.

Interestingly, our results showed that the inclusion of heavy ions—unique to K-H vortices occurring at Mars—serves to reduce γ, but increase Ω_{KH}. However, we emphasize that K-H vortices may occur even with a reduced γ, as nonlinear development depends not only upon the local growth rate but also the initial upstream solar wind perturbation. γ decreases because the bulk velocities of the heavy ions are low, reducing the free energy per mass density. On the other hand, heavy ions also serve to lower the stabilizing effect of the induced magnetospheric magnetic field. This causes the most K-H stable direction to lean toward the magnetosheath's magnetic field direction, shrinking the solid angle over which the boundary is stable. In an extreme case, if the Alfvén speed on the induced magnetospheric side is zero, then the entire plane perpendicular to the magnetosheath's magnetic field direction becomes K-H unstable (i.e., $\mathbf{k} \cdot \mathbf{B} = 0$) as long as there is a flow shear in that plane. This stands in stark contrast to earlier arguments regarding the stabilizing effect of heavy ions in the growth of K-H modes. Rather, our study strongly suggests that planetary heavy ions play a more complex role in allowing for "easier" initiation and development of K-H instability.

The results above demonstrate that the uniqueness of Mars' plasma environment and magnetic field morphology (i.e., absence of an intrinsic magnetosphere and presence of planetary heavy ions) does not necessarily inhibit or restrict the onset and growth of K-H instability. On the contrary, there is a significant likelihood of instability occurring anywhere along the IMB, at any given time, as long as there exists a direction wherein the maximum growth rate is sufficiently high to initiate K-H instability modes. The increased "ease" of K-H onset due to heavy ions could also explain the vortices observed at the equatorial flanks and southern hemisphere. In fact, heavy ions have been shown to similarly lower the threshold for K-H onset at Earth's magnetopause (Bouhram et al., 2005). Overall, our study suggests a higher occurrence frequency, and hence, a larger contribution to global atmospheric loss from K-H vortices than previously assumed.

3.3. Loss of Atmospheric Oxygen

Previous works (e.g., Penz et al., 2004) have illustrated the important role that K-H vortices could play as an eroding force on the Martian ionosphere. The loss of atmospheric oxygen resulting from the detachment of the vortex structure, along with embedded planetary heavy ions, represents the putative final stage of K-H development.

Following the back-of-the-envelope calculation outlined in Brace et al. (1982) and Poh et al. (2021), we estimated instantaneous loss rates for the six events in this work. We modeled the vortices as a cylindrical structure, with a diameter equivalent to the K-H wavelength (see Section 3) and a length of ~1 R_{Mars}. To estimate the number of planetary ions n (O^+ or $O_2{}^+$) carried by such a vortex cloud, we use $n = \rho_{pl} V$ where the density of planetary ions ρ_{pl} is the mean of O^+ and $O_2{}^+$ number densities, and V is the volume of the cylinder. Using the number of vortices in each wave train as a (lower bound) estimate of the global number of vortices occurring along the IMB at any given time, we then estimated the instantaneous loss rate by dividing the total number of planetary ions carried across all vortices by the estimated K-H period.

Our calculations (Table 1) show instantaneous loss rates of planetary ions ranging from 10^{25} to 10^{27} s^{-1}, comparable to previous empirical estimates (i.e., 5.0 $\times$ 10^{25} s^{-1} in X. Wang et al. (2022) and 5.9 $\times$ 10^{26} s^{-1} in Poh et al. (2021)). Given the higher global occurrence rates inferred in this study, our estimates challenge previous assumptions (Poh et al., 2021) that instantaneous loss rates derived empirically may range higher than actual globally integrated rates. Although the occurrence, growth, and detachment of K-H vortices is neither a continuous nor omnipresent process, it is clear that the contribution of K-H vortices to overall Martian atmospheric escape is more significant than previously thought. The relaxation of onset conditions for K-H instability significantly extends the spatial domain in which vortices can develop to the flanks and southern hemisphere, instead of being restricted to the northern hemisphere as previously assumed. To address whether higher occurrence rates could result in atmospheric loss rates rivaling or surpassing other escape mechanisms (e.g., atmospheric sputtering), we require a better quantification of the occurrence frequency of K-H waves.

4. Summary and Conclusion

In summary, our findings significantly advance our understanding of K-H vortices at Mars as follows:

1. We analyzed six observations of fully developed K-H vortices. Each K-H vortex is identified and analytically confirmed by characteristic plasma and magnetic field signatures such as quasi-periodic, sawtooth-like magnetic field perturbations.
2. We presented, to the best of our knowledge, the first observations of K-H vortices along the IMB in the equatorial flanks and southern terminator regions. Our results suggest that the spatial domain in which K-H instability occurs is larger than previously thought.
3. We estimated the linear growth rate of K-H vortices observed to be 10^{-2}–10^{-3} s^{-1}. We determined that the most K-H unstable direction is largely in the tailward direction, and that the solid angle over which the flow shear boundary is unstable to K-H onset is ∼26%–74% of all directions. We concluded that the inclusion of heavy planetary ions at Mars reduces the growth rate, but increases the solid angle over which K-H instability occurs. Our results strongly support a higher occurrence rate for K-H vortices than previously assumed.
4. We estimated the instantaneous ion loss rate from our K-H events to be $\sim 10^{25}$–10^{27} s^{-1}. Combined with higher occurrence rates over a larger spatial region, we concluded that atmospheric loss due to the detachment of K-H vortices at Mars could be more significant than previous estimates.

Our results challenge the validity of prior assumptions regarding the nature of K-H instability—specifically its onset and growth—when applying our understanding at Earth to Mars, given stark differences in their plasma and magnetic field morphology. This significantly impacts previous, more conservative estimates of atmospheric loss rates caused by detached plasma clouds. Further statistical studies are required to better quantify loss rates from K-H vortices, and their contribution to Mars' overall atmospheric escape. Given recent developments in deep learning techniques, future work could include the development of an automated routine to expand upon the statistics of K-H vortex occurrence.

Acknowledgments
Support for this work is provided by NASA's Planetary Science Division Research Program, through ISFM work package Exospheres, Ionospheres, Magnetospheres Modeling at Goddard Space Flight Center. The MAVEN project is supported by NASA through the Mars Exploration Program, and provided support for G. P., K. G. H., J. E., and G. DB. Z. K. and G. P. are supported through a cooperative agreement with Center for Research and Exploration in Space Sciences and Technology II (CRESST II) between NASA Goddard Space Flight Center and Catholic University of America under Award 80GSFC24M0006, and NASA Discovery Data Analysis Program (DDAP) Grant 80NSSC21K1012. X.M. is supported by NASA Grants 80NSSC18K1108 and 80NSSC23K0899, as well as NSF Grants 2308853 and DOE Grant DE-SC0022952. D.C.P. is supported by NASA Grant 80GFSC21M0002.

Conflict of Interest

The authors declare no conflicts of interest relevant to this study.

Data Availability Statement

The instrument data (MAG, SWIA, SWEA, and STATIC) from MAVEN analyzed in this study are publicly available and archived with the NASA Planetary Data System (PDS) (https://pds-ppi.igpp.ucla.edu/mission/MAVEN). A Python-based data analysis tool for MAVEN was developed for the purpose of this study and can be found at https://github.com/kohzewen/pymaven.

References

Adamson, E., Nykyri, K., & Otto, A. (2016). The Kelvin–Helmholtz instability under Parker-spiral interplanetary magnetic field conditions at the magnetospheric flanks. *Advances in Space Research*, *58*(2), 218–230. https://doi.org/10.1016/j.asr.2015.09.013

Amerstorfer, U. V., Erkaev, N. V., Taubenschuss, U., & Biernat, H. K. (2010). Influence of a density increase on the evolution of the Kelvin–Helmholtz instability and vortices. *Physics of Plasmas*, *17*(7), 072901. https://doi.org/10.1063/1.3453705

Azari, A. R., Abrahams, E., Sapienza, F., Halekas, J., Biersteker, J., Mitchell, D. L., et al. (2024). A virtual solar wind monitor at Mars with uncertainty quantification using Gaussian processes. *Journal of Geophysical Research: Machine Learning and Computation*, *1*(3), e2024JH000155. https://doi.org/10.1029/2024JH000155

Blasl, K. A., Nakamura, T. K. M., Plaschke, F., Nakamura, R., Hasegawa, H., Stawarz, J. E., et al. (2022). Multi-scale observations of the magnetopause Kelvin–Helmholtz waves during southward IMF. *Physics of Plasmas*, *29*(1), 012105. https://doi.org/10.1063/5.0067370

Boardsen, S. A., Sundberg, T., Slavin, J. A., Anderson, B. J., Korth, H., Solomon, S. C., & Blomberg, L. G. (2010). Observations of Kelvin-Helmholtz waves along the dusk-side boundary of Mercury's magnetosphere during MESSENGER's third flyby. *Geophysical Research Letters*, *37*(12), L12101. https://doi.org/10.1029/2010GL043606

Bouhram, M., Klecker, B., Paschmann, G., Haaland, S., Hasegawa, H., Blagau, A., et al. (2005). Survey of energetic O^+ ions near the dayside mid-latitude magnetopause with cluster. *Annales Geophysicae*, *23*(4), 1281–1294. https://doi.org/10.5194/angeo-23-1281-2005

Brace, L., Theis, R., & Hoegy, W. (1982). Plasma clouds above the ionopause of Venus and their implications. *Planetary and Space Science*, *30*(1), 29–37. https://doi.org/10.1016/0032-0633(82)90069-1

Chandrasekhar, S., & Gillis, J. (1962). Hydrodynamic and hydromagnetic stability. *Physics Today*, *15*(3), 58. https://doi.org/10.1063/1.3058072

Connerney, J. E. P., Espley, J. R., DiBraccio, G. A., Gruesbeck, J. R., Oliversen, R. J., Mitchell, D. L., et al. (2015). First results of the MAVEN magnetic field investigation. *Geophysical Research Letters*, *42*(21), 8819–8827. https://doi.org/10.1002/2015GL065366

Dang, T., Lei, J., Zhang, B., Zhang, T., Yao, Z., Lyon, J., et al. (2022). Oxygen ion escape at Venus associated with three-dimensional Kelvin-Helmholtz instability. *Geophysical Research Letters*, *49*(6), e2021GL096961. https://doi.org/10.1029/2021GL096961

Delamere, P. A., Barnes, N. P., Ma, X., & Johnson, J. R. (2021). The Kelvin-Helmholtz instability from the perspective of hybrid simulations. *Frontiers in Astronomy and Space Sciences*, *8*, 211. https://doi.org/10.3389/fspas.2021.801824

Delamere, P. A., Wilson, R. J., Eriksson, S., & Bagenal, F. (2013). Magnetic signatures of Kelvin-Helmholtz vortices on Saturn's magnetopause: Global survey. *Journal of Geophysical Research: Space Physics*, *118*(1), 393–404. https://doi.org/10.1029/2012JA018197

Delamere, P. A., Wilson, R. J., & Masters, A. (2011). Kelvin-Helmholtz instability at Saturn's magnetopause: Hybrid simulations. *Journal of Geophysical Research*, *116*(A10), A10222. https://doi.org/10.1029/2011JA016724

DiBraccio, G. A., Dann, J., Espley, J. R., Gruesbeck, J. R., Soobiah, Y., Connerney, J. E. P., et al. (2017). MAVEN observations of tail current sheet flapping at Mars. *Journal of Geophysical Research: Space Physics*, *122*(4), 4308–4324. https://doi.org/10.1002/2016JA023488

DiBraccio, G. A., Espley, J. R., Gruesbeck, J. R., Connerney, J. E. P., Brain, D. A., Halekas, J. S., et al. (2015). Magnetotail dynamics at Mars: Initial MAVEN observations. *Geophysical Research Letters*, *42*(21), 8828–8837. https://doi.org/10.1002/2015GL065248

Eriksson, S., Lavraud, B., Wilder, V., Stawarz, J. E., Giles, B. L., Burch, J. L., et al. (2016). Magnetospheric multiscale observations of magnetic reconnection associated with Kelvin-Helmholtz waves. *Geophysical Research Letters*, *43*(11), 5606–5615. https://doi.org/10.1002/2016GL068783

Fairfield, D. H., Otto, A., Mukai, T., Kokubun, S., Lepping, R. P., Steinberg, J. T., et al. (2000). Geotail observations of the Kelvin-Helmholtz instability at the equatorial magnetotail boundary for parallel northward fields. *Journal of Geophysical Research*, *105*(A9), 21159–21173. https://doi.org/10.1029/1999JA000316

Halekas, J. S., Brain, D. A., Ruhunusiri, S., McFadden, J. P., Mitchell, D. L., Mazelle, C., et al. (2016). Plasma clouds and snowplows: Bulk plasma escape from Mars observed by MAVEN. *Geophysical Research Letters*, *43*(4), 1426–1434. https://doi.org/10.1002/2016GL067752

Halekas, J. S., Taylor, E. R., Dalton, G., Johnson, G., Curtis, D. W., McFadden, J. P., et al. (2015). The solar wind ion analyzer for MAVEN. *Space Science Reviews*, *195*(1–4), 125–151. https://doi.org/10.1007/s11214-013-0029-z

Hasegawa, H. (2012). Structure and dynamics of the magnetopause and its boundary layers. *Monographs on Environment, Earth and Planets*, *1*(2), 71–119. https://doi.org/10.5047/meep.2012.00102.0071

Hasegawa, H., Fujimoto, M., Phan, T., Rème, H., Balogh, A., Dunlop, M., et al. (2004). Transport of solar wind into Earth's magnetosphere through rolled-up Kelvin–Helmholtz vortices. *Nature*, *430*(7001), 755–758. https://doi.org/10.1038/nature02799

Hasegawa, H., Retinò, A., Vaivads, A., Khotyaintsev, Y., André, M., Nakamura, T. K. M., et al. (2009). Kelvin-Helmholtz waves at the Earth's magnetopause: Multiscale development and associated reconnection. *Journal of Geophysical Research*, *114*(A12), A12207. https://doi.org/10.1029/2009JA014042

Jakosky, B. M., Grebowsky, J. M., Luhmann, J. G., & Brain, D. A. (2015). Initial results from the MAVEN mission to Mars. *Geophysical Research Letters*, *42*(21), 8791–8802. https://doi.org/10.1002/2015GL065271

Kavosi, S., & Raeder, J. (2015). Ubiquity of Kelvin-Helmholtz waves at Earth's magnetopause. *Nature Communications*, *6*(1), 7019. https://doi.org/10.1038/ncomms8019

Ma, X. (2023). Estimation of the Kelvin–Helmholtz unstable boundary. *Journal of Geophysical Research: Space Physics*, *128*(8), e2023JA031602. https://doi.org/10.1029/2023JA031602

Masters, A., Achilleos, N., Cutler, J., Coates, A., Dougherty, M., & Jones, G. (2012). Surface waves on Saturn's magnetopause. *Planetary and Space Science*, *65*(1), 109–121. https://doi.org/10.1016/j.pss.2012.02.007

Masters, A., Achilleos, N., Kivelson, M. G., Sergis, N., Dougherty, M. K., Thomsen, M. F., et al. (2010). Cassini observations of a Kelvin-Helmholtz vortex in Saturn's outer magnetosphere. *Journal of Geophysical Research*, *115*(A7), A07225. https://doi.org/10.1029/2010JA015351

McFadden, J. P., Livi, R., Luhmann, J., Connerney, J., Mitchell, D. L., Mazelle, C., et al. (2015). Structure of the Martian ionosphere: MAVEN STATIC first results. In *AAS/AGU triennial earth-sun summit* (Vol. 1, p. 209.04).

Mitchell, D. L., Mazelle, C., Sauvaud, J. A., Thocaven, J. J., Rouzaud, J., Fedorov, A., et al. (2016). The MAVEN solar wind electron analyzer. *Space Science Reviews*, *200*(1–4), 495–528. https://doi.org/10.1007/s11214-015-0232-1

Nykyri, K., Otto, A., Lavraud, B., Mouikis, C., Kistler, L. M., Balogh, A., & Rème, H. (2006). Cluster observations of reconnection due to the Kelvin-Helmholtz instability at the dawnside magnetospheric flank. *Annales Geophysicae*, *24*(10), 2619–2643. https://doi.org/10.5194/angeo-24-2619-2006

Penz, T., Erkaev, N., Biernat, H., Lammer, H., Amerstorfer, U., Gunell, H., et al. (2004). Ion loss on Mars caused by the Kelvin–Helmholtz instability. *Planetary and Space Science*, *52*(13), 1157–1167. https://doi.org/10.1016/j.pss.2004.06.001

Poh, G., Espley, J. R., Nykyri, K., Fowler, C. M., Ma, X., Xu, S., et al. (2021). On the growth and development of non-linear Kelvin–Helmholtz instability at Mars: MAVEN observations. *Journal of Geophysical Research: Space Physics*, *126*(9), e2021JA029224. https://doi.org/10.1029/2021JA029224

Ruhunusiri, S., Halekas, J. S., McFadden, J. P., Connerney, J. E. P., Espley, J. R., Harada, Y., et al. (2016). MAVEN observations of partially developed Kelvin-Helmholtz vortices at Mars. *Geophysical Research Letters*, *43*(10), 4763–4773. https://doi.org/10.1002/2016GL068926

Russell, C. T., & Elphic, R. C. (1979). Observation of magnetic flux ropes in the Venus ionosphere. *Nature*, *279*(5714), 616–618. https://doi.org/10.1038/279616a0

Smith, A. W., Slavin, J. A., Jackman, C. M., Poh, G.-K., & Fear, R. C. (2017). Flux ropes in the Hermean magnetotail: Distribution, properties, and formation. *Journal of Geophysical Research: Space Physics*, *122*(8), 8136–8153. https://doi.org/10.1002/2017JA024295

Sonnerup, B. U. Ö., & Scheible, M. (1998). Minimum and maximum variance analysis. *ISSI Scientific Reports Series*, *1*, 185–220.

Sundberg, T., Boardsen, S. A., Slavin, J. A., Blomberg, L. G., Cumnock, J. A., Solomon, S. C., et al. (2011). Reconstruction of propagating Kelvin–Helmholtz vortices at Mercury's magnetopause. *Planetary and Space Science*, *59*(15), 2051–2057. https://doi.org/10.1016/j.pss.2011.05.008

Taylor, M. G. G. T., Hasegawa, H., Lavraud, B., Phan, T., Escoubet, C. P., Dunlop, M. W., et al. (2012). Spatial distribution of rolled up Kelvin-Helmholtz vortices at Earth's dayside and flank magnetopause. *Annales Geophysicae*, *30*(6), 1025–1035. https://doi.org/10.5194/angeo-30-1025-2012

Terada, N., Machida, S., & Shinagawa, H. (2002). Global hybrid simulation of the Kelvin–Helmholtz instability at the Venus ionopause. *Journal of Geophysical Research*, *107*(A12), SMP30-1–SMP30-20. https://doi.org/10.1029/2001JA009224

Thomas, V. A., & Winske, D. (1991). Kinetic simulation of the Kelvin-Helmholtz instability at the Venus ionopause. *Geophysical Research Letters*, *18*(11), 1943–1946. https://doi.org/10.1029/91GL02552

Wang, L., Huang, C., Du, A., Ge, Y., Chen, G., Yang, Z., et al. (2023). Kelvin-Helmholtz instability at Mars: In situ observations and kinetic simulations. *The Astrophysical Journal*, *947*(2), 51. https://doi.org/10.3847/1538-4357/acc655

Wang, X., Xu, X., Ye, Y., Wang, J., Wang, M., Zhou, Z., et al. (2022). MAVEN observations of the Kelvin-Helmholtz instability developing at the ionopause of Mars. *Geophysical Research Letters*, *49*(7), e2022GL098673. https://doi.org/10.1029/2022GL098673

Wolff, R. S., Goldstein, B. E., & Yeates, C. M. (1980). The onset and development of Kelvin-Helmholtz instability at the Venus ionopause. *Journal of Geophysical Research*, *85*(A13), 7697–7707. https://doi.org/10.1029/JA085iA13p07697

Erratum

The originally published version of this article neglected to include the authors' full names. The authors' names have been corrected as follows: Ze-Wen Koh, Gangkai Poh, Christopher M. Fowler, Kathleen Gwen Hanley, Xuanye Ma, Jacob R. Gruesbeck, Dona Chathuni P. Kuruppuaratchi, Weijie Sun, Gina A. DiBraccio, and Jared Randolph Espley. This may be considered the authoritative version of record.